Electron paramagnetic resonance on iron-acceptor pairs in silicon

J. J. van Kooten, G. A. Weller, and C. A. J. Ammerlaan
Natuurkundig Laboratorium der Universiteit van Amsterdam, Valckenierstraat 65, 1018-XE Amsterdam, The Netherlands
(Received 6 June 1984)

Experimental data obtained by electron paramagnetic resonance on silicon doped with aluminum and iron are presented. After quenching the sample and a short stay at room temperature, two spectra, labeled Si-NL27 and Si-NL28, were observed. It is concluded that the spectra originate from two Fe-Al pairs with different symmetry. The spectra can be described with an effective spin $J=\frac{1}{2}$ and g factors significantly deviating from 2. A theoretical investigation of the g-value tensors of iron-acceptor pairs allows an interpretation of the g factors in terms of crystal-field splitting and spin-orbit coupling.

INTRODUCTION

Because of its high solubility and diffusion coefficient[1] iron often is unintentionally present as an impurity in silicon crystals. The preferential position of iron is the interstitial T site. After quenching the crystal from 1200 °C the iron concentration can be as high as 2×10^{16} cm^{-3}. Because of its low migration energy [0.69 eV (Ref. 1)] iron is readily involved in defect reactions. Examples are the clustering of iron and iron-acceptor pairing.[2,3] These reactions take place even at room temperature. Iron-acceptor pairs are electrically active and their levels have been determined by deep-level transient spectroscopy.[2,3] The electrical donor level of iron in the band gap is at $E_v+0.38$ eV.[2] It is noted that there are two levels belonging to Fe-Al (Refs. 2 and 3) whereas other iron-acceptor pairs have just one electrical level.

The microscopic structure of many transition-metal—acceptor pairs is known from the extensive work of Ludwig and Woodbury.[4] All such impurity pairs show the same configuration: a substitutional negatively charged acceptor with the positively charged transition metal in a ⟨111⟩ direction. The only exception is Fe-In where the iron ion is aligned along a ⟨001⟩ direction. The most probable position of the metal ion is the nearest, or in the case of Fe-In, the next-nearest interstitial T site to the acceptor ion. Since the acceptor ion has a closed shell of electrons, its main effect on the transition-metal ion is to disturb its cubic environment.

Except for Fe-Ga all the electron paramagnetic resonance (EPR) spectra of the pairs can be described with g values near the free-electron value, i.e., $g=2$. Regarding iron, Ludwig and Woodbury reported the EPR spectra of pairs formed with B, Ga, and In.[4] More recently the EPR of Fe-B was investigated in more detail by Gehlhoff and Segsa.[5]

EXPERIMENTAL PROCEDURE

The samples were p-type Al-doped silicon with 1 Ω cm resistivity and typical dimensions $2\times2\times20$ mm^3. Starting material for all samples was float-zone dislocation-free Wacker WASO silicon. Iron was diffused into the sample by enclosing the sample together with a piece of iron in an open quartz ampoule. Before this the iron was etched in HCl and the silicon sample was ground and etched. In order to diffuse ^{57}Fe, the sample and ampoule were coated with a $^{57}FeCl_3$ solution. The ampoule with the sample was heated to 1200 °C for about 1 h and then quenched in water. The SiO_2 which was formed was removed by HF, and after another etch the sample was stored in liquid nitrogen.

The EPR spectra were measured on a superheterodyne K-band spectrometer. The sample was mounted with a ⟨011⟩ direction perpendicular to the magnetic field. The measurements were taken at 4.2 K in dispersion mode. The results were reproduced in four samples.

RESULTS

Immediately after quenching two new spectra were observed in addition to the familiar isotropic spectra of Fe_i^0 at $g=2.070$ and Fe_i^+ at $g=3.524$.[4] The new spectra are labeled Si-NL27 and Si-NL28. The very anisotropic spectra NL27 and NL28 have respectively, a trigonal and rhombic I symmetry. The angular-dependent resonance patterns are shown in Figs. 1 and 2. Both spectra showed a sixfold splitting caused by hyperfine interactions with one Al nucleus (nuclear spin $I=\frac{5}{2}$, abundance 100%). In spectrum NL28 an additional twofold splitting appeared in the samples doped with iron enriched to 90% in the magnetic isotope ^{57}Fe (nuclear spin $I=\frac{1}{2}$). The hyperfine splittings due to Al and Fe are small and of comparable magnitude, resulting in overlapping of various resonances. Only in some favorable directions was a well-resolved splitting observed, as shown in Fig. 3. Unfortunately it was not possible to measure the complete angular dependence of the hyperfine splittings.

The fine structure of both spectra could be analyzed with the simple spin Hamiltonian $H=\mu_B\vec{B}\cdot\vec{\vec{g}}\cdot\vec{J}$ with $J=\frac{1}{2}$. The appropriate g values were determined by a computer fit and are listed in Table I.

After keeping the samples for one night (17 h) at room temperature the isolated iron impurity spectra had disap-

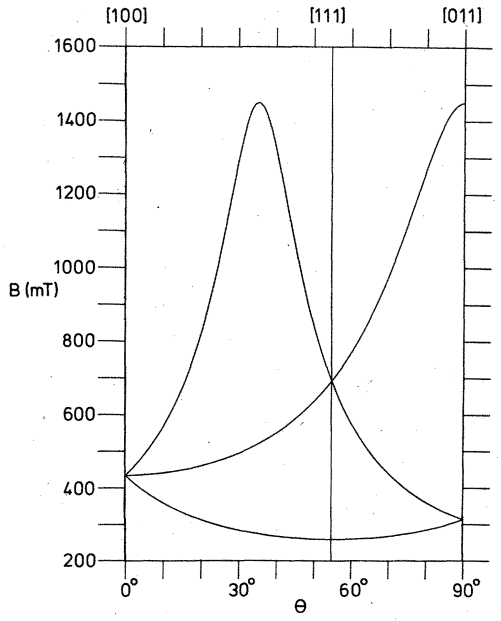

FIG. 1. Angular dependence, $\vec{B}$ in the $(0\bar{1}1)$ plane, of spectrum Si-NL27 corresponding to the trigonal Fe-Al pair.

peared and NL27 and NL28 had gained in intensity by about a factor of 3. Heating successively for 1 h to temperatures of 50, 70, and 90 °C destroys the spectra. The annealing characteristics of NL27 and NL28 are schematically represented in Fig. 4.

MODEL

The observed hyperfine structure of spectrum NL28 clearly indicates the involvement of one iron and one aluminum atom in the paramagnetic center. Since Al is substitutionally incorporated in the silicon lattice and iron diffuses interstitially we propose that NL28 corresponds to Fe_iAl_s. As the point-group symmetry of the center is

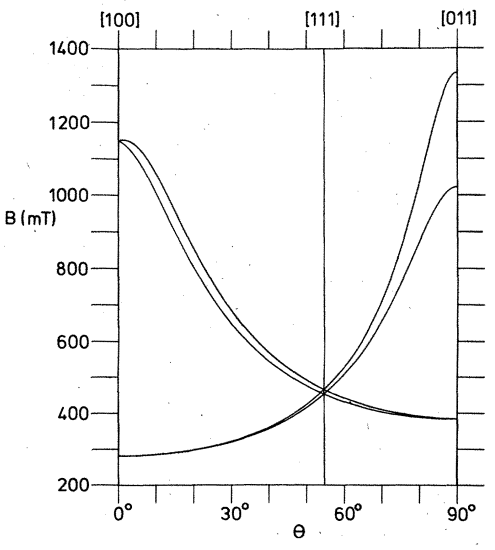

FIG. 2. Angular dependence, $\vec{B}$ in the $(0\bar{1}1)$ plane, of spectrum Si-NL28 corresponding to the rhombic *I* Fe-Al pair.

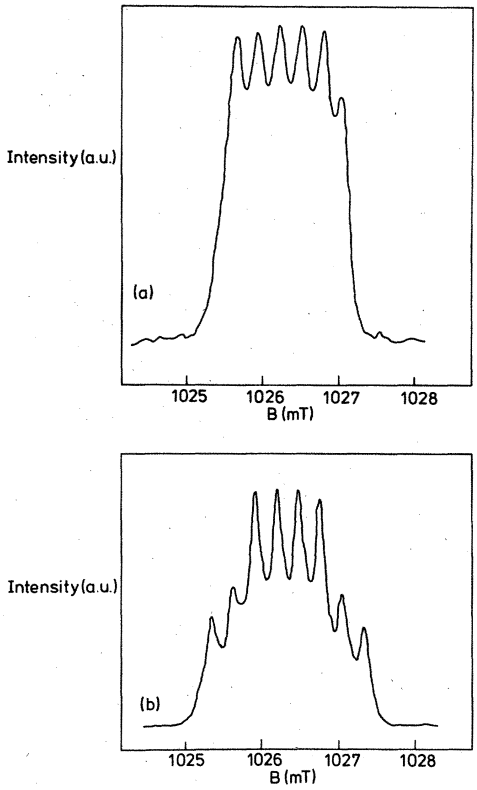

FIG. 3. Line shape of spectrum NL28, for $\vec{B}||[011]$, showing the hyperfine structure due to ^{27}Al (a) and to additional ^{57}Fe (b).

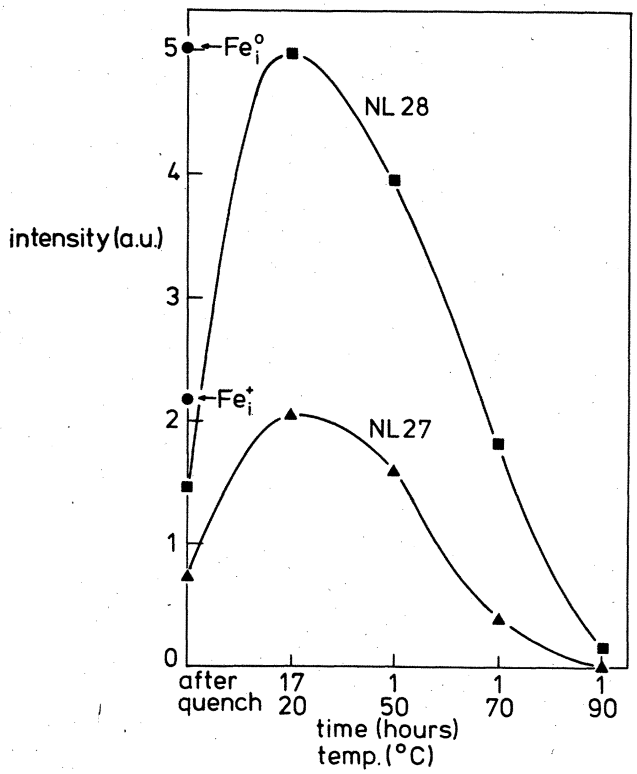

FIG. 4. Annealing characteristics of the EPR spectra NL27 and NL28.

TABLE I. Principal g values and directions of the EPR spectra Si-NL27 and Si-NL28.

Spectrum	Symmetry	g_1	g_2	g_3
NL27	Trigonal	6.389±0.003 ∥[111]	1.138±0.005 ⊥[111]	1.138±0.005 ⊥[111]
NL28	Rhombic I	5.885±0.001 ∥[100]	1.236±0.001 ∥[011]	1.612±0.001 ∥[0$\bar{1}$1]

2 *mm* the iron atom must be along a ⟨001⟩ axis passing through the Al atom. Most likely the iron atom is to be found on the next-nearest interstitial T position to the Al atom.

In the case of NL27 the hyperfine splitting from Al was observed contrary to that of ^{57}Fe. However, in view of the diffusion characteristics and annealing behavior we also identify NL27 with an Fe_iAl_s impurity pair. In this case the iron atom occupies a site on a ⟨111⟩ axis as seen from the aluminum atom, probably close to the nearest interstitial T position. The two atomic models are shown in Figs. 5 and 6. As was mentioned, the angular dependence of the hyperfine interactions with the aluminum was not measured. Nevertheless, from the observed splittings of about 0.3 mT the spin density on the acceptor nucleus may be estimated to be less than 1%. This small value indicates that the aluminum is essentially in the negative charge state. The model of an ionic pair Fe_i^+-Al_s^- is thereby confirmed.

ANALYSIS

The vast majority of EPR spectra of point defects in silicon has a g value very close to the free-electron splitting factor i.e., $g=2$. The reason is that in these defects the electron orbital momentum is strongly quenched by crystal forces. The presence of orbital momentum in transition metals in silicon is understood by the phenomenological model of Ludwig and Woodbury.[4] The spectra of Fe-Al as well as Fe-Ga (Ref. 4) show, even when fitted with a spin higher than $\frac{1}{2}$, rather uncommon g factors. This section gives a model of the electronic structure of iron-acceptor pairs by which the observed g values can be interpreted in terms of crystal fields and spin-orbit coupling.

An iron-acceptor pair consists of a negatively charged substitutional acceptor and a positively charged iron atom at an interstitial position. The electronic configuration of the iron ion is $3d^7$. In the free ion the lowest term is ^4F followed by ^4P at about 1.38 eV (Ref. 6). Other terms are of no importance. For iron in a silicon lattice on an interstitial T site the cubic crystal field splits the lowest term into two orbital triplets and a singlet as shown in Fig. 7. We will confine our calculations to the lowest triplet. Within this triplet we can define a fictitious orbital momentum $\vec{l}\,',l'=1$ with components l'_x,l'_y,l'_z (Ref. 7). The axial and rhombic crystal fields and the spin-orbit coupling are given by the Hamiltonian:

$$H=H_{\rm cr}+H_{\rm s.o.} \tag{1a}$$

with

$$H_{\rm cr}=\Delta_{\rm ax}(1-l_z'^2)+\Delta_{\rm rh}(l_x'^2-l_y'^2)\,, \tag{1b}$$

$$H_{\rm s.o.}=\lambda\vec{L}'\vec{S}=-\lambda(\alpha_x l'_x S_x+\alpha_y l'_y S_y+\alpha_z l p'_z S_z)\,, \tag{1c}$$

with $\vec{L}'$ the effective orbital momentum, $-\alpha_x,-\alpha_y,-\alpha_z$ the effective Landé factors of the triplet, and λ the spin-orbit coupling constant and spin $S=\frac{3}{2}$. This leads to a splitting into six Kramers doublets, as indicated in Fig. 7. Application of a magnetic field $\vec{B}$, lifting the remaining degeneracy, is accounted for by the Zeeman Hamiltonian $H_z=\mu_B\vec{B}\cdot(\vec{L}'+2\vec{S})$. The lowest doublet can be regarded as a doublet with effective spin $J=\frac{1}{2}$. The effect of the external magnetic field is then described by the effective Hamiltonian $H_{\rm eff}=\mu_B\vec{B}\cdot\overleftrightarrow{g}\cdot\vec{J}$, with an effective g tensor $\overleftrightarrow{g}$.

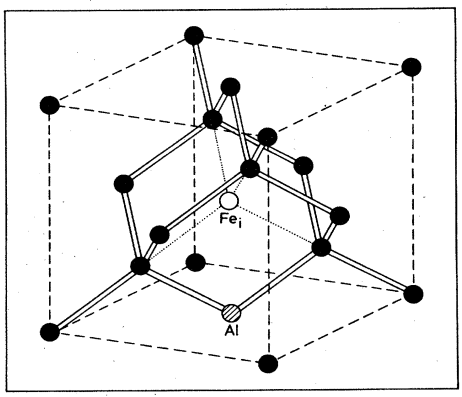

FIG. 5. Atomic model of the Fe_i-Al_s pair corresponding to EPR spectrum NL28.

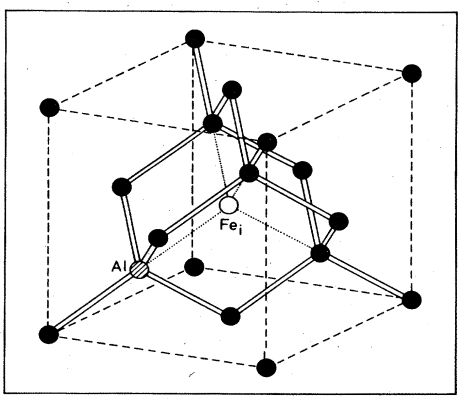

FIG. 6. Atomic model of the Fe_i-Al_s pair corresponding to EPR spectrum NL27.

TABLE II. Matrix elements of the crystalline field and the spin-orbit coupling in the $^4\Gamma_4$ state.

		$\|-x,+\frac{3}{2}\rangle$ $\|x,-\frac{3}{2}\rangle$	$\|iy,+\frac{3}{2}\rangle$ $\|iy,-\frac{3}{2}\rangle$	$\|-x,-\frac{1}{2}\rangle$ $\|x,+\frac{1}{2}\rangle$	$\|iy,-\frac{1}{2}\rangle$ $\|iy,+\frac{1}{2}\rangle$	$\|z,-\frac{3}{2}\rangle$ $\|z,+\frac{3}{2}\rangle$	$\|z,+\frac{1}{2}\rangle$ $\|z,-\frac{1}{2}\rangle$
$\langle -x,+\frac{3}{2}\|$	$\langle x,-\frac{3}{2}\|$	δ_{rh}	$\frac{3}{2}$	0	0	0	$\frac{1}{2}\sqrt{3}$
$\langle -iy,+\frac{3}{2}\|$	$\langle -iy,-\frac{3}{2}\|$	$\frac{3}{2}$	$-\delta_{rh}$	0	0	0	$\frac{1}{2}\sqrt{3}$
$\langle -x,-\frac{1}{2}\|$	$\langle x,+\frac{1}{2}\|$	0	0	δ_{rh}	$-\frac{1}{2}$	$\frac{1}{2}\sqrt{3}$	-1
$\langle -iy,-\frac{1}{2}\|$	$\langle -iy,+\frac{1}{2}\|$	0	0	$-\frac{1}{2}$	$-\delta_{rh}$	$\frac{1}{2}\sqrt{3}$	1
$\langle z,-\frac{3}{2}\|$	$\langle z,+\frac{3}{2}\|$	0	0	$\frac{1}{2}\sqrt{3}$	$\frac{1}{2}\sqrt{3}$	δ_{ax}	0
$\langle z,+\frac{1}{2}\|$	$\langle z,-\frac{1}{2}\|$	$\frac{1}{2}\sqrt{3}$	$\frac{1}{2}\sqrt{3}$	-1	1	0	δ_{ax}

CALCULATIONS

We restricted our calculations to the orbital triplet Γ_4 and a spin quartet. The orbital part of the wave functions is denoted by $|x\rangle, |y\rangle, |z\rangle$ and the spin part by $|+\frac{3}{2}\rangle, |+\frac{1}{2}\rangle, |-\frac{1}{2}\rangle, |-\frac{3}{2}\rangle$. The 12-dimensional matrix of the Hamiltonian (1) with respect to these basis states can be reduced to two identical six-dimensional matrices because of Kramers degeneracy. To facilitate the calculations the number of parameters is reduced by considering the special case with $\alpha_x=\alpha_y=\alpha_z=\alpha$. Dimensionless quantities are introduced by defining $\delta_{ax}=\Delta_{ax}/\alpha\lambda$ and $\delta_{rh}=\Delta_{rh}/\alpha\lambda$. The matrix elements are then found as given in Table II. Eigenvalues and eigenfunctions of Hamiltonian (1) as a function of the parameters δ_{ax} and δ_{rh} are calculated by computer diagonalization of this matrix. The lowest doublet can be written as

$$|+\rangle=a\,|-x,+\tfrac{3}{2}\rangle+b\,|iy,+\tfrac{3}{2}\rangle+c\,|-x,-\tfrac{1}{2}\rangle+d\,|iy,-\tfrac{1}{2}\rangle+e\,|z,-\tfrac{3}{2}\rangle+f\,|z,+\tfrac{1}{2}\rangle\,, \tag{2a}$$

$$|-\rangle=a\,|x,-\tfrac{3}{2}\rangle+b\,|iy,-\tfrac{3}{2}\rangle+c\,|x,+\tfrac{1}{2}\rangle+d\,|iy,+\tfrac{1}{2}\rangle+e\,|z,+\tfrac{3}{2}\rangle+f\,|z,-\tfrac{1}{2}\rangle\,. \tag{2b}$$

The Zeeman splitting factors are then calculated to be

$$g_x=2\langle+|(L_x+2S_x)|-\rangle=|-4c^2+4d^2+4f^2-(4\sqrt{3})ac+(4\sqrt{3})bd+(4\sqrt{3})ef+\alpha(4be+4df)|\,, \tag{3a}$$

$$g_y=2i\langle+|(L_y+2S_y)|-\rangle=4c^2-4d^2+4f^2-(4\sqrt{3})ac+(4\sqrt{3})bd-(4\sqrt{3})ef-\alpha(4ae+4cf)|\,, \tag{3b}$$

$$g_z=2\langle+|(L_z+2S_z)|+\rangle=|6a^2+6b^2-2c^2-2e^2+2f^2+\alpha(4ab+4cd)|\,. \tag{3c}$$

The terms containing the effective Landé factor α are contributions of the orbital moment to the magnetic splitting. The other terms are arising from the spin part of the wave function. Neglecting covalency, α is determined by the admixture of $^4\Gamma_4(^4P)$ to the ground state $^4\Gamma_4(^4F)$. We have taken $\alpha=\frac{3}{2}$, corresponding with no admixture of ^4P orbitals. For very large cubic fields the admixture is 20%, which results in $\alpha=1$ representing the minimum value of α in this model.

Figures 8 and 9 show the relation between the g components for various values of the axial field δ_{ax} and rhombic field δ_{rh}. The calculations contain two limiting cases for which analytical solutions can be given.

(a) Axial field only. This case is represented by the solid curve in Fig. 8. The numerical result is in agreement with the calculations of Abragam and Pryce.[8] For the present case of $\alpha=\frac{3}{2}$, the theoretical expressions which they derived are summarized by

$$g_x=g_y=\frac{4(x^4+7x^3+22x^2+24x)}{(x^4+4x^3+18x^2+24x+24)}\,, \tag{4a}$$

$$g_z=2-\frac{14(x^2-12x-12)}{(x^4+4x^3+18x^2+24x+24)}\,, \tag{4b}$$

where the positive variable x is related to the axial crystal field by

$$\Delta_{ax}=3\lambda\frac{(x^3+5x^2-8x-12)}{4(x^2+2x)}\,. \tag{4c}$$

(b) Both axial and rhombic fields much larger than the spin-orbit coupling, leading to an isolated ground-state quartet. This situation can equivalently be described with an effective spin $J=\frac{3}{2}$ and a zero-field splitting spin Hamiltonian term:

TABLE III. Comparison between experimental and theoretical g factors for iron-acceptor pairs in silicon.

			Experiment			Theory					
Model	Symmetry	Reference	g_x	g_y	g_z	g_x	g_y	$\frac{g_x+g_y}{2}$	g_z	Δ_{ax} (eV)	Δ_{rh} (eV)
Fe-B	Trigonal	5	4.090	4.090	2.068	4.090	4.090		1.999	−1.421	0
Fe-Al	Trigonal	This work	1.138	1.138	6.389	1.266	1.011	1.138	6.390	0.862	0.151
Fe-Al	Rhombic I	This work	1.236	1.612	5.885	1.238	1.611		5.885	1.579	0.390
Fe-Ga	Trigonal	4	2.530	2.530	5.087	3.192	1.868	2.530	5.087	0.487	0.276
Fe-In	Rhombic I	4	3.780	4.400	2.070	3.784	4.396		1.985	−1.331	0.068

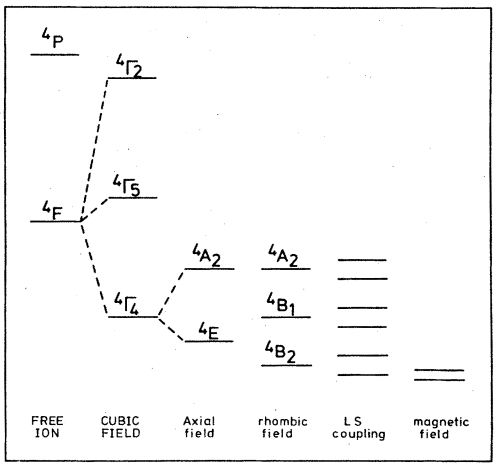

FIG. 7. Energy-level scheme for the $Fe^+(3d^7)$ ion.

$$H_{zf}=DJ_z^2+E(J_x^2-J_y^2)\ . \tag{4d}$$

The g factors for the lowest doublet in the $J=\frac{1}{2}$ formalism are then given by[9]

$$g_x=\left|2-\frac{(2D-6E)}{(D^2+3E^2)^{1/2}}\right|\ , \tag{5a}$$

$$g_y=\left|2-\frac{(2D+6E)}{(D^2+3E^2)^{1/2}}\right|\ , \tag{5b}$$

$$g_z=\left|2+\frac{4D}{(D^2+3E^2)^{1/2}}\right|\ . \tag{5c}$$

The zero-field splitting arises from second-order perturbation of the spin-orbit interaction of the crystal-field levels. The parameters D and E are related to the basic parameters by

$$D=-\alpha^2\lambda^2\frac{\Delta_{ax}}{\Delta_{ax}^2-\Delta_{rh}^2}\ ,$$
$$E=-\alpha^2\lambda^2\frac{\Delta_{rh}}{\Delta_{ax}^2-\Delta_{rh}^2}\ . \tag{6}$$

The ratio between E and D is just the ratio between the rhombic and axial crystal field: $E/D=\Delta_{rh}/\Delta_{ax}$. This case is represented in Fig. 8 by the dotted curve.

Those parts of the curves near $(g_x,g_y,g_z)=(4,4,2)$ correspond to a large positive axial field, a ground-state orbital singlet, and completely quenched orbital momentum. The well-known case of strong axial field, effective spin $J=\frac{3}{2}$ leading to $g_{\|}=2$ and $g_{\perp}=4$ applies. The lower right parts in Figs. 8 and 9 correspond to a large negative axial field where an orbital doublet constitutes the ground state. Here still some orbital contribution can be induced in the axial component of the g tensor. It may enhance the value of g_z from the spin-only value $g_z=6$ to a maximum of $g_z=9$. Changing the sign of the rhombic potential only interchanges g_x with g_y.

It may be verified that the experimental data are close

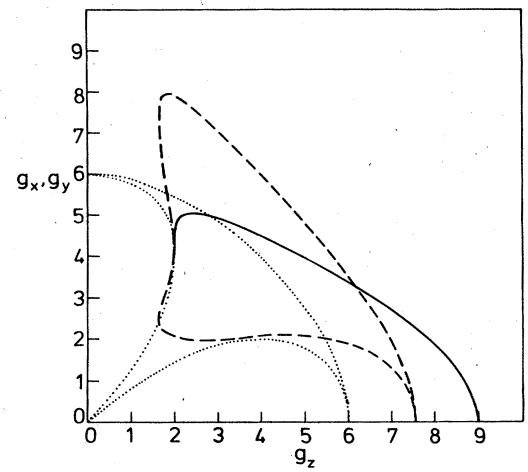

FIG. 8. The Zeeman splitting factors g_x, g_y, and g_z as a function of the axial field for rhombic field $\delta_{rh}=0$(——), 2.5(— — —), or ∞ (. . . .).

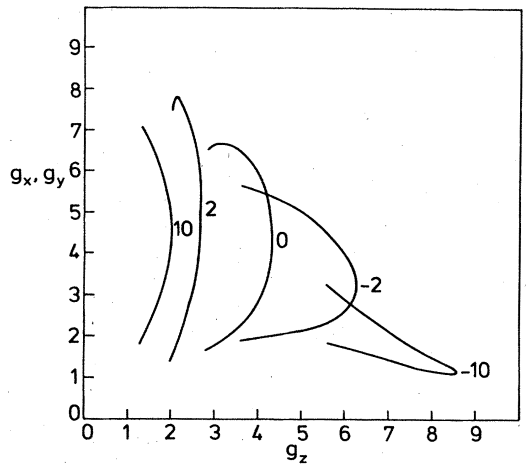

FIG. 9. Zeeman splitting factors g_x, g_y, and g_z as a function of the rhombic field δ_{rh} ($-5<\delta_{rh}<5$) for five values of the axial field.

to the curve explained in case (b). The rhombic spectra of Fe-In and Fe-Al can be fitted by a proper choice of δ_{ax} and δ_{rh}. The values of Δ_{ax} and Δ_{rh}, as given in Table III, were calculated using $\alpha=\frac{3}{2}$ and $\lambda=-14.26$ meV.[10] We cannot account for the small discrepancy in the z component of g in Fe-In. As for the axial spectra we note from Figs. 8 and 9 that it is impossible to fit the spectra of Fe-Ga and Fe-Al with an axial field only corresponding to case (a) and the theory of Abragam and Pryce. A reduction of the effective Landé factor to $\alpha=1$ represents too small an improvement. The empirical value $\alpha=0.25$ does account fairly well for the experimental data of the axial spectra. This, however, is an unrealistic choice. When $\Delta_{ax}<0$ the doublet has the lowest energy. This orbitally degenerate state is unstable because of the Jahn-Teller effect and the system will distort to monoclinic or triclinic symmetry. The theory of Abragam and Pryce is therefore expected not to be applicable to the lower right of point $(4\frac{1}{3},4\frac{1}{3},4\frac{1}{3})$. Since in the experiment axial symmetry is observed one is forced to assume that in fact the system is rapidly hopping from one stable distorted configuration to another. By motional averaging one then detects an axial symmetric spectrum. We can fit the spectra of Fe-Al and Fe-Ga with a rhombic field by taking $g_\perp=\frac{1}{2}(g_x+g_y)$ and $g_{||}=g_z$. By fitting the data of the spectra with a field of rhombic symmetry the extra degree(s) of freedom present in the actual monoclinic (triclinic) symmetry is not exploited. The results are listed in Table III. Again a good agreement between the experimental and theoretical g tensor is achieved. No chemical trend is apparent in the crystal fields for the various acceptor ions.

Interstitial positive Fe_i^+ represents the special case in which both the axial and rhombic crystal fields vanish. In the remaining cubic crystalline field the ground state is an orbital triplet which also is liable to Jahn-Teller distortion. The quenching of the orbital contribution to the g factor was discussed by Ham.[11] He showed that dynamical effects can account for the reduction of the g factor from the isotropic value $g=4\frac{1}{3}$, as indicated in Figs. 8 and 9, to the value $g=3.524$ which is actually observed.

CONCLUSIONS

Applying magnetic resonance spectroscopy two iron-aluminium pairs with a different symmetry were revealed. Their spectra Si-NL27 and Si-NL28 complement the earlier results of Ludwig and Woodbury on iron-acceptor pairs. The anisotropic g-factors of iron-acceptor pairs can be understood with the model presented in this paper based on crystal fields and spin-orbit couplings. It is proposed that the axial spectra of Fe-Al and Fe-Ga are in fact the motionally averaged spectra associated with centers of lower symmetry.

ACKNOWLEDGMENTS

The authors want to thank R. van Kemp and M. Sprenger for their experimental assistance and E. G. Sieverts for theoretical discussions. This research was supported by the Foundation for Fundamental Research of Matter (Stichting voor Fundamenteel Onderzoek der Materie), The Netherlands.

[1]E. R. Weber, Appl. Phys. A **30**, 1 (1983).
[2]K. Wünstel and P. Wagner, Appl. Phys. A **27**, 207 (1982).
[3]K. Graff and H. Pieper, J. Electrochem. Soc. **128**, 669 (1981).
[4]G. W. Ludwig and H. H. Woodbury, in *Solid State Physics*, edited by F. Seitz and D. Turnbull (Academic, New York, 1962), Vol. 13 p. 223.
[5]W. Gehlhoff and K. H. Segsa, Phys. Status Solidi B **115**, 443 (1983).
[6]C. E. Moore, *Atomic Energy Levels*, Natl. Bur. Stand. (U.S.) Circ. No. 467 (U.S. G.P.O., Washington, D.C., 1979), Vol. II.
[7]A. Abragam and M. H. L. Pryce, Proc. R. Soc. London, Ser. A **205**, 135 (1951).

[8]A. Abragam and M. H. L. Pryce, Proc. R. Soc. London, Ser. A **206**, 173 (1951).
[9]J. C. M. Henning, J. Liebertz, and R. P. van Stapele, J. Phys. Chem. Solids **28**, 1109 (1967).
[10]T. M. Dunn, Trans. Faraday Soc. **57**, 1441 (1961).
[11]F. S. Ham, in *Electron Paramagnetic Resonance,* edited by S. Geschwind (Plenum, New York, 1972).